

A Mid Mesozoic Revolution in the regulation of ocean chemistry

ANDY RIDGWELL

Department of Earth and Ocean Sciences, University of British Columbia, Vancouver, British Columbia

Corresponding author:

Andy Ridgwell

*Department of Earth and Ocean Sciences,
The University of British Columbia,
6339 Stores Road,
Vancouver, British Columbia V6T 1Z4
Canada
Tel: 604-827-5793
Fax: 604-822-6088
Email: aridgwell@eos.ubc.ca*

Revised for: Marine Geology

October 2004

Abstract

The Phanerozoic has seen fundamental changes in the global biogeochemical cycling of calcium carbonate (CaCO_3), particularly the advent of biomineralization during the early Cambrian when the products of weathering could first be removed through metabolic expenditure, and the subsequent ecological success of planktic calcifiers during the Mesozoic which shifted the locus of deposition from the continental shelves to the deep open ocean. These biologically-driven CaCO_3 depositional ‘mode’ changes along with geochemical and tectonic variations in boundary conditions such as sea-level and calcium ion concentrations all affected the carbonate chemistry of the ocean. I employ a model of atmosphere-ocean-sediment carbon cycling to explore the impact of these factors on the saturation state and carbonate chemistry of the global ocean during the Phanerozoic.

The model results highlight that overall; the time evolution and regulation of Phanerozoic ocean chemistry is dominated by a Mid Mesozoic Revolution in the marine carbonate cycle. Prior to this transition, it was possible for the ocean to attain states of extreme saturation during the Permian and Triassic as well as during the late Precambrian. This is primarily a consequence of low sea-level in restricting the potential area for the deposition of shallow water carbonates, thus requiring a more saturated ocean and higher rate of precipitation per unit area is then required in order to balance weathering input. This is consistent with the occurrence of mineralogically ‘anomalous’ carbonates during these periods but not commonly at other times. That the modern carbon cycle does not respond to similar tectonic forcings is due to the ecological success of calcifying planktic taxa during the Mesozoic, which in facilitating the creation of a responsive deep-sea carbonate sink enabled a much greater degree of regulation of saturation state than was

previously possible. The model results also highlight the primary role of changes in the concentration of CO₂ in the atmosphere and of Ca²⁺ in the ocean in determining surface pH. The uncertainty inherent in paleo CO₂ estimates then translates into sufficient uncertainty in reconstructions of Phanerozoic temperature variability that one can only deduce from the carbonate δ¹⁸O record that the Cretaceous was generally warmer and the Carboniferous colder than average. The substantially enhanced oceanic carbon inventory predicted for the Paleozoic suggests that previous calculations of methane hydrate release may have substantially underestimated the quantity of clathrate carbon required to explain observed carbon isotopic excursions. In both cases the importance of quantifying Phanerozoic marine chemistry is clear.

Keywords: Phanerozoic; carbon cycle; calcium carbonate; ocean chemistry

1. Introduction

The geological record reveals considerable variability inherent in Phanerozoic climate. Some intervals have been characterized by repeated and/or long-lived ice ages while other times have apparently remained ice-free [Crowell, 1999; Crowley, 1998]. Linked to this, indicators of global temperature exhibit what has been viewed as a first-order oscillation between ‘warm’ and ‘cool’ modes of the climate system [Frakes *et al.*, 1992; Royer *et al.*, 2004; Veizer *et al.*, 2000].

Although there has been recent controversy regarding the most important driver for this change [Rahmstorf *et al.*, 2004; Royer *et al.*, 2004; Shaviv and Veizer, 2003], variations in the concentration of CO₂ in the atmosphere is very likely to be a key causative factor. Analysis of the evolution of global carbon cycling through the Phanerozoic has therefore tended to focus only on the factors that control atmospheric CO₂ on geologic time-scales; silicate rock weathering and CO₂ out-gassing from metamorphic sources together with the erosion of ancient kerogens and burial of new organic matter [Berner, 1990, 1992, 1994; Franck *et al.*, 1999, 2000; Tajika, 1998, 1999]. Changes taking place in the marine carbonate cycle, here taken to include the speciation of dissolved CO₂ and ambient pH together with the cycling of CaCO₃ between ocean and surficial sediments, have been considered unimportant in this context [Franck *et al.*, 2000].

The evolution of the marine carbonate cycle is, however, central to understanding the regulation of ocean chemistry through the Phanerozoic. The occurrence of extremes of ocean over-saturation may be critical in understanding the driving forces behind the evolution of carbonate biomineralizing species [Walker *et al.*, 2002]. Surface ocean saturation state also provides the environmental context for the geological interpretation of primary carbonate

mineralogy, particularly the occurrence of abundant environmentally controlled carbonates [Grotzinger and Knoll, 1995; Riding, 1993] as well as observed shifts in the relative abundance of calcite and aragonite [Mackenzie and Morse, 1992; Sandberg, 1983; Stanley and Hardie, 1998, 1999; Wilkinson *et al.*, 1984]. Of central importance in the control of saturation state is the ‘mode’ of carbonate deposition [Sumner and Grotzinger, 1996]; here taken to include; the degree of biotic vs. abiotic control on carbonate production and the primary locus of deposition and preservation in the marine environment.

Understanding global carbonate cycling takes on additional importance because saturation state is one of the factors that along with atmospheric CO₂ and oceanic Ca²⁺ concentrations co-determines bulk ocean carbonate chemistry and pH. Knowledge of the concentration of dissolved inorganic carbon or alkalinity is a prerequisite in the interpretation of carbonate δ¹¹B in terms of surface CO₂ partial pressure [Pearson and Palmer, 1999a, 2000]. Similarly, pH must be known in order to remove fractionation effects if past climate states are to be reconstructed from carbonate δ¹⁸O [Royer *et al.*, 2004]. The inventory of dissolved inorganic carbon in the ocean (and atmosphere) is also a required given in mass-balance interpretation of δ¹³C excursions [Dickens *et al.*, 1995; Jiang *et al.*, 2003; Kennedy *et al.*, 2001; Rothman *et al.*, 2003].

The existence and potential significance of mode changes in carbonate deposition during the Phanerozoic have long been recognized in the context of deep-water vs. shallow-water carbonate sinks [Berger and Winterer, 1974; Riding, 1993] (Figure 1). Quantitative analysis of the impact of evolutionary events such as the proliferation of calcareous plankton taxa (Figure 1a) and how this interacts with tectonic forcings has not previously been made. I therefore explore the implications for Phanerozoic ocean chemistry of changes in a number of the key

forcings of the system; planktic calcite production, sea-level and the extent of epeiric seas, oceanic Ca^{2+} concentrations, and weathering rates. Quantitative reconstruction of how the key metrics of marine chemistry and carbonate cycling respond to these forcings is made with the aid of a numerical model of atmosphere-ocean-sediment carbon cycling.

2. Modelling strategy

2.1 Background

The geochemical or long-term carbon cycle primarily involves the exchange of carbon between the ‘geologic’ and ‘surficial’ reservoirs, the latter comprising atmosphere, oceans, biosphere, and soils [Berner and Caldeira, 1997] and to which can be added the exchangeable surface sediments, particularly those located in the deep-sea. Imbalances induced in the carbon fluxes between these two reservoirs do not drive unbounded oscillations in surficial carbon inventory because atmospheric CO_2 is ultimately regulated through silicate weathering feedback [Berner and Caldeira, 1997]. The time-scale for this is of order 100 kyr to 1 Myr, depending on whether the coupled CaCO_3 depositional feedback is taken into account [Sundquist, 1991; Ridgwell and Kennedy, 2004]. Thus, the first requirement for a suitable numerical model tool is to be able to access time-scales of >100 kyr. Rather unhelpfully, the short-term carbon cycle, which involves the partitioning of carbon within the surficial ocean-atmosphere-biosphere-soil-sediment system operates much quicker. In particular, the process of air-sea gas exchange which links the surface ocean with the atmosphere requires a time step of order months for numerical stability of the model. Clearly, use of a relatively spatially under-resolved ‘box’ model representation of the ocean (e.g., Broecker and Peng, 1986; Caldeira and Rampino, 1993; Sundquist, 1990) rather

than an ocean general circulation model (e.g., *Archer* [1996b]) is highly advantageous. Traceability of model formulation and validation is also an important consideration, and there is little point in continually re-inventing the wheel. A model previously employed in comparative analysis of modern vs. Neoproterozoic modes of CaCO_3 cycling [*Ridgwell et al.*, 2003; *Ridgwell and Kennedy*, 2004] is therefore chosen as the basis for this present study.

2.2 Model description

The ocean component of the model is based on the ‘PANDORA’ ocean carbon cycle box model of *Broecker and Peng* [1986]. This is shown schematically in Figure 2a. The physical structure of the ocean together with prescribed ocean circulation and export fluxes of particulate organic carbon (POC) are taken directly from *Broecker and Peng* [1986]. Remineralization of POC in the water column is parameterized as a simple exponential decay curve with an *e*-folding depth of 500 m together with a residual flux of ‘recalcitrant’ organic matter set at 8% of the initial export flux [*Ridgwell*, 2001], producing an oceanic distribution of $[\text{PO}_4^{3-}]$ near identical to PANDORA. For planktic carbonate export, an *e*-folding depth of 10,000 m is chosen to replicate the PANDORA dissolution distribution. The ocean surface is coupled to a ‘well-mixed’ atmosphere with a prescribed air-sea CO_2 gas transfer coefficient of $0.061 \text{ mol m}^{-2} \text{ yr}^{-1} \mu\text{atm}^{-1}$ [*Maier-Reimer*, 1993]. Below, the ocean is coupled to a representation of the preservation and burial of CaCO_3 in deep sea sediments [*Ridgwell*, 2001; *Ridgwell et al.*, 2002]. All particulate organic matter reaching the sediment surface is assumed to be completely oxidized with no loss occurring through burial.

Each of the ocean surface boxes is coupled to an idealized representation of shallow water (neritic) carbonate deposition [*Caldeira and Rampino*, 1993; *Munhoven and François*,

1996; *Ridgwell et al.*, 2003]. In this scheme, the strength of the CaCO_3 sink is assumed to be in direct proportion to total depositional area available such that the accumulation rate of carbonate is given by; $f\text{CaCO}_3 = A \times \lambda \times (\Omega_{(\text{aragonite})} - 1)^n$. The saturation state or solubility ratio, Ω is defined as $[\text{Ca}^{2+}] \times [\text{CO}_3^{2-}] / K_{\text{sp}}$, where K_{sp} is a solubility constant (see *Zeebe and Wolf-Gladrow* [2001]). The neritic area, A is determined by integrating the surface area of the Earth flooded above the depth of the shelf break, taken to be 200 m to make the depositional scheme comparable with that of *Munhoven and François* [1996]. λ is a global scaling factor for neritic carbonate production and n is a ‘process’ power. Although the linking of precipitation rate to saturation state draws from abiotic system understanding [*Burton and Walter*, 1987], individual corals and reef communities have also been shown to exhibit a dependence of calcification rate on Ω [*Leclercq et al.*, 2000; *Marshall and Clode*, 2002]. I set $n = 1.7$ consistent with observed latitudinal relationships between shallow-water carbonate accumulation rates and sea-surface saturation state [*Opdyke and Wilkinson*, 1993].

For pelagic carbonate production in the open ocean, rather than assume a spatially uniform export ratio of CaCO_3 to POC, I use the same saturation-dependent formulation as for the neritic environment to link CaCO_3 flux with the local saturation state; $f\text{CaCO}_3 = f\text{POC} \times \gamma \times (\Omega_{(\text{calcite})} - 1)^n$, where $f\text{POC}$ is the prescribed POC flux (molC yr^{-1}) in PANDORA, γ is a global scaling factor for planktic carbonate production, and $n = 1.7$ as before. Linking export CaCO_3 :POC to saturation in this way enables a reasonable simile of the modern sediment surface % CaCO_3 distribution to be achieved (not shown) when deployed within the framework of a 3D ocean circulation model [*Hargreaves et al.*, in press]. The underlying justification is that planktic calcifiers such as coccolithophores, like corals, also exhibit a dependence of calcification on ambient carbonate ion concentrations [*Riebesell et al.*, 2000]. However, the model results are not

particularly sensitive to the details of this function because it is the preservational response of CaCO_3 in deep-sea sediments rather than changes in production *per se* that dominates the global burial rate response [Archer, 2003].

Loss of dissolved inorganic carbon (DIC) and alkalinity (ALK) from the marine environment as a result of sedimentary burial of CaCO_3 must be balanced on the long-term by the out-gassing of CO_2 in conjunction with the weathering of terrigenous rocks. The riverine supply rate of HCO_3^- derived from silicate weathering in the modern system is assumed to be 12 TmolC yr^{-1} , a figure generally consistent with a range of studies (see *Munhoven* [2002] and references therein). The HCO_3^- flux from the weathering of carbonates is initially set at 18 TmolC yr^{-1} [*Munhoven*, 2002]. No account is taken of the erosion of sedimentary kerogen.

It should be recognized that while the depositional rate of CaCO_3 in both pelagic and neritic depositional environments is locally controlled by ambient saturation, steady-state must ultimately be achieved with total global deposition balancing the solute input to the ocean. Thus, on a global basis and on time-scales much longer than the ca. 5-10 kyr adjustment time of the marine carbonate cycle, burial of CaCO_3 is dictated by the weathering flux of HCO_3^- to the ocean. It is the rate of weathering in conjunction with modifying factors such as the total available area for neritic deposition which then dictates ocean Ω . Thus, the model is in a sense a rather glorified numerical means for solving for ocean saturation state given that the total sedimentation flux must balance total weathering flux and that the sedimentation flux a function of Ω .

The model is initially configured for the modern carbon cycle and mode of carbonate deposition. With a total HCO_3^- weathering input to the ocean of 30 TmolC yr^{-1} , steady-state carbonate burial must be 15 TmolC yr^{-1} . Of this, 10 TmolC yr^{-1} is assumed to occur in the deep-

sea consistent with model and observational estimates [Archer, 1996b; Milliman *et al.*, 1999; Milliman and Droxler, 1996]. A combination of numerical (implicit) and ‘trial-and-error’ methods are used to determine the values of the two carbonate production rate scaling factors γ (0.097) and λ (0.038) required to achieve a 2:1 partitioning of CaCO_3 burial between deep-sea and neritic sedimentary environments. The system is additionally constrained to have a pre-industrial atmospheric CO_2 concentration of 278 ppm and a mean ocean ALK close to the modern value of 2374 $\mu\text{mol eq kg}^{-1}$ [Yamanka and Tajika, 1996]. Mean surface $\Omega_{(\text{calcite})}$ and ocean DIC are then 5.4 and 2227 $\mu\text{molC kg}^{-1}$, respectively. The predicted distribution of wt% CaCO_3 in deep-sea sediments is shown in Figure 2b. An inter-basin fractionation of CaCO_3 accumulation in deep-sea sediments is correctly reproduced [Archer, 1996a; Berger and Winterer, 1974] with a progressive decrease in the maximum depth to which CaCO_3 accumulates in the sediments from Atlantic basin, through (Indo-) Pacific to North Pacific (along with sub-Antarctic and Southern Ocean). However, there are deficiencies in the details, such as too much CaCO_3 preservation at depth in the Atlantic and insufficient in the Pacific compared to observations [Archer, 1996a]. However, at 33%, the fractional preservation of CaCO_3 in deep-sea sediments globally is only slightly higher than the 20-30% range that data-driven analysis suggests [Archer, 1996b]. The model also demonstrates an appropriate sensitivity of the marine carbonate cycle to perturbation – the injection of 500 GtC DIC for instance, results in an initial increase in atmospheric CO_2 from 278 to 314 ppm followed by decay to 295 ppm on a time-scale of ca. 8 kyr as the deep-sea sediments adjust. The uncompensated and carbonate compensated CO_2 responses of the box model (36 and 17 ppm, respectively) are reassuringly close to that predicted by a 3D ocean general circulation model based geochemical model – 37 and 17 ppm,

respectively [Archer *et al.*, 2000], giving confidence that the behavior of the marine carbonate cycle is being captured appropriately.

2.3 Model application

Having configured the model for the present-day, a series of time-slices are created spanning the Phanerozoic. There is no ‘memory’ of previous time-slice states (i.e., no hysteresis) and because final steady-state is independent of the starting conditions the model can equally be run either forwards or backwards in time with each subsequent time-slice taking its initial conditions from the end of the previous one. I choose backwards in time because the initial conditions of the modern system are known *a priori* whereas those characterizing the early Phanerozoic are not. (Note that it is possible to make an estimate of the prevailing late Precambrian ocean chemistry given a climatic constraint on atmospheric CO₂ and carbonate mineralogical constraint on ocean Ω [Ridgwell and Kennedy, 2004].) An interval of 20 Myr between time-slices is chosen as sufficient to delineate secular change in the modes of carbonate deposition without incurring an undue computational burden. The length of integration for each time-slice is set at 250 kyr, sufficient to achieve near steady-state under all eventualities. Thus, in addition to the modern simulation, 10 – 550 Ma is spanned by 28 separate 250 kyr time-slices with each experiment therefore representing a total of 7 Myr of numerical integration carried out at a 3-month time-step. The need for a simplified geochemical ‘box’ model is obvious.

The traditional approach to modeling long-term carbon cycling is exemplified by Robert Berner’s highly influential ‘GEOCARB’ model for Phanerozoic CO₂ [Berner, 1990, 1992, 1994; Berner and Kothavala, 2001]. The name of the game here is to calculate the concentration of CO₂ in the atmosphere necessary to drive a silicate rock weathering rate sufficient to balance

metamorphic CO₂ out-gassing. Additional CO₂ inputs resulting from any excess in the rate of ancient kerogen erosion over burial of new organic matter must also be taken into account.

Rather than populate the World with yet another clone of GEOCARB I take a different approach and assume that the value of atmospheric CO₂ is known. Although the scatter in proxy CO₂ estimates is substantial [Royer *et al.*, 2004] there is sufficient data to estimate the magnitude of the uncertainty (Figure 3a). The concentration of atmospheric CO₂ in the model is then continually restored to the data-derived CO₂ value for each 20 Myr time-slice rather than being left free to find its own level as in GEOCARB. This avoids having to make estimates of past rates of CO₂ out-gassing and of the erosion and burial of organic carbon. For time-slices earlier than 410 Ma when little proxy CO₂ data is available I substitute the values calculated by GEOCARB III [Berner and Kothavala, 2001, Royer *et al.*, 2004]. To explore the sensitivity of the results to assumed CO₂, the model experiments are run not only with the mean CO₂ value but also with ± 1 standard deviation. Additional forcings of global carbonate cycling that are applied are; sea-level, the concentration of Ca²⁺ in the ocean, and weathering rates, shown in Figures 3b, 3c, and 3d, respectively. These are described briefly below.

(i) Sea-level. The Phanerozoic has seen secular oscillation in eustatic sea-level of in excess of 300 m [Hallam, 1984; Haq *et al.*, 1988] (Figure 3b). Occurrence of high sea-level such as the Early-to-Mid Paleozoic resulted in typical flooding extents of 20-50% of total cratonic area [Algeo and Sleslavinsky, 1995]. These times of extensive epeiric seas are associated with widespread carbonate platform development and shallow carbonate accumulation in general [Boss and Wilkinson, 1991; Opdyke and Wilkinson, 1988; Walker *et al.*, 2002]. What proportion of the global area of shallow seas is conducive to substantive long-term carbonate accumulation is not so simple to calculate however. Ambient ocean surface temperature is an important factor

[*Burton and Walter, 1987; Opdyke and Wilkinson, 1993*] and can change in response to climate as well as paleo-latitude [*Walker et al., 2002*]. Nutrient availability (oligotrophic status [*Wood, 1993*]) and the prevailing erosive and sediment transport regimes will also play a role. Finally, but not least, tectonic subsidence and the creation of accommodation space exerts a critical control [*Jacquin and Vail, 1995*]. However, because weathering must be balanced on the long-term by carbonate deposition taking place *somewhere*, regardless of the details of the environment at any one location, a general inverse relationship between global shallow water area and precipitation rate per unit area (directly related to ocean saturation) is inescapable. Varying sea-level and re-calculating the depositional area as total cratonic area flooded above a fixed base elevation of -200 m will then give a measure of the impact of Phanerozoic sea-level on ocean saturation state. Note that the global scaling factor, λ implicitly accounts for carbonate deposition taking place over just a fraction of total shallow sea floor area. What it cannot do however is account for a change in this fraction, such as due to a climatically-driven shift in the maximum latitudinal limits of coral growth.

(ii) Ca^{2+} . Analysis of fluid inclusions contained in halite crystals of marine origin reveals a substantial Phanerozoic variability in Calcium ion concentrations ($[\text{Ca}^{2+}]$) [*Horita et al., 2002; Lowenstein et al., 2001, 2003*]. This has important implications for the carbonate chemistry of the ocean because $[\text{Ca}^{2+}]$ and $[\text{CO}_3^{2-}]$ are inversely related through the solubility ratio $\Omega = [\text{Ca}^{2+}] \times [\text{CO}_3^{2-}] / K_{\text{sp}}$. For constant ocean saturation (read: constant precipitation rate per unit area) a change in ambient $[\text{Ca}^{2+}]$ will push $[\text{CO}_3^{2-}]$ in the opposite direction. The time-history of the $[\text{Ca}^{2+}]$ forcing of the model is taken from the reconstruction of *Stanley and Hardie [1998]* and consistent with recent measurements made by *Horita et al. [2002]* and *Lowenstein et al. [2003]* (Figure 3c).

(iii) Weathering. Without an unambiguous proxy, estimation of past changes in rock weathering rates and the supply of solutes to the ocean is difficult. I employ the results of GCM based simulations spanning the last 237 Myr that took into account the relevant changes in paleogeography, paleoclimate, and paleogeology [Gibbs *et al.*, 1999]. The spread of results arising from different assumptions made in weathering formulation and prevailing atmospheric CO₂ concentration then provides a measure of the uncertainty in estimated weathering rates. The relative change in the total HCO₃⁻ flux of Gibbs *et al.* [1999] is used to scale the present-day solute supply rate of 30 TmolC yr⁻¹ assumed in the model here. Prior to 237 Ma which is the oldest time-slice considered by Gibbs *et al.* [1999], weathering rates are simply set equal to modern.

3. The impact of changes in the mode of carbonate deposition

The role of the global carbonate cycle in the evolution of Phanerozoic ocean chemistry is highlighted with a series of sensitivity experiments. Common to all the model experiments are applied variations in atmospheric CO₂ (Figure 3a), sea-level (Figure 3b), oceanic [Ca²⁺] (Figure 3c), and weathering input (Figure 3d). Where they differ is in the assumed importance of pelagic carbonate production in the open ocean. In the first experiment the model is run under a modern mode of carbonate cycling with delivery of CaCO₃ to deep-sea sediments in addition to neritic deposition (Section 3.2) – referred to from here onwards as the ‘Cretan’ ocean mode [Zeebe and Westbroek, 2003]. In the second experiments, CaCO₃ deposition is assumed restricted to shallow water environments only – a ‘Neritan’ ocean [Zeebe and Westbroek, 2003]. The final experiment considers a scenario in which the primary locus of carbonate deposition shifts from shallow seas to the deep ocean in response to the proliferation of calcareous plankton in the open ocean

(Section 3.3). Because there is no hysteresis in the model this can be achieved in practice by splicing together results drawn from the previous two experiments.

3.1 Phanerozoic ocean chemistry in a ‘Cretan’ ocean

The behavior of the Cretan ocean is shown in Figure 4. The saturation state as represented by mean surface Ω_{calcite} is well regulated. Only during the early Paleozoic does surface Ω deviate by more than ± 0.5 from the modern value of ~ 5.4 . Uncertainty in weathering rate (the shaded limits in the figure) increases the amplitude of the variability, but saturation is still reasonably constrained about modern. The contribution to overall variability due to the uncertainty in atmospheric CO₂ is not included, but translates into little more than an additional ± 0.1 in the maximum spread of values.

In contrast, surface pH (Figure 4b) undergoes substantial change during the Phanerozoic with a secular oscillation of up to ± 0.4 superimposed on an underlying increase of ~ 0.6 pH units. Uncertainty in estimated pH is dominated by atmospheric CO₂, and the contribution due to the uncertainty in weathering rate (not included) represents only an additional ± 0.05 pH.

Finally, Figure 4c illustrates how the global steady state burial flux of CaCO₃ is partitioned. The total burial flux conforms, as it must, to the imposed weathering time-history (Figure 3d). The neritic component reflects both the variability in total input (weathering) as well as a modulation due to sea-level and the area of shallow water depositional environments. The sea-level component of the variability in neritic burial becomes obvious prior to 230 Ma when the weathering rate is fixed at modern.

3.2 Phanerozoic ocean chemistry in a ‘Neritan’ ocean

The Neritan ocean responds to the applied forcings very differently (Figure 5). While the $p\text{H}$ curve still resembles the Cretan ocean, saturation state is now extremely variable, with extremes in Ω_{calcite} of 9–11 reached in the Permian and Triassic as well as under present-day boundary conditions. The apparently poor regulation of saturation state is also reflected in the much greater spread in saturation driven by the uncertainty in weathering. Now, rather than ca. -0.6 to +0.3 limits, the Neritan ocean exhibits uncertainty limits of ca. -2.0 to +1.0 about the mean forcing response.

3.3 The impact of plankton ecological succession

In the Cretan ocean, the planktic carbonate factory and associated deep-sea sedimentary sink plays a key role in the stabilization of the marine carbon cycle. Ocean saturation state is well regulated and the impact of two-fold variability in continental weathering rates (Figure 3d), three-fold variability in oceanic $[\text{Ca}^{2+}]$ (Figure 3c), and more than three-fold variability in the area of shallow seas driven by sea-level (Figure 3b) is muted. In contrast, the strong negative deep-sea preservational feedback on ocean saturation is absent in the ‘Neritan’ Earth system and carbonate chemistry is much less well regulated [Zeebe and Westbroek, 2003].

The establishment of a well-regulated marine carbonate cycle and introduction of a ‘Cretan’ ocean can be viewed as a two-step change in the mode of carbonate deposition [Sumner and Grotzinger, 1996]; (1) the advent of biomineralization around the time of the Cambrian–Precambrian boundary [Wood *et al.*, 2002], and (2) the Mesozoic proliferation of planktic calcifiers [Martin, 1995]. In the first step, evolutionary innovation conferred on life the ability to precipitate carbonate structures (skeletons) and directly drive the removal of weathering products from the ocean. Prior to this there would have been no significant biologically driven production

of CaCO_3 , with carbonate deposition restricted to heterogeneous nucleation and crystal growth on organic and inorganic surfaces in predominantly warm shallow water environments. While inorganic-physiochemical spontaneous precipitation of calcite or aragonite crystals ('whittings') in the open ocean represents a potential source of carbonate to deep-sea sediments, the geochemical conditions required are rather extreme. Spontaneous (homogeneous) nucleation in sea water solutions is not experimentally observed until $\Omega_{\text{cal}} > \sim 20 - 25$ [Morse and He, 1993] and it is only in relatively localized freshwater environments and even higher degrees of over-saturation that apparently inorganic-physiochemical whittings occur [Arp *et al.*, 1999]. The impact of 'switching on' biomineralization would be a fall in the degree of over-saturation as metabolic expenditure is used to help drive the precipitation of CaCO_3 at a faster rate than could occur by abiotic mechanisms alone. The imbalance of carbonate sinks over weathering thereby induced would be corrected and steady-state re-established once carbonate accumulation globally returned to the same rate as prior to the advent of biomimetic mineralization, but now requiring a less over-saturated ocean. We could potentially represent this transition in the model by turning the appropriate 'knob' in the model (λ). What a realistic change in parameter value might be and how quickly it might have changed with time is not obvious. We will therefore focus our attention on the second, Mesozoic transition in this paper.

While there is some evidence for the presence of planktic biomimetic mineralizers around the time of the Silurian or even Ordovician it is not until the Mid Mesozoic that a marked proliferation in coccolithophore and foraminifera diversity and abundance is observed [Boss and Wilkinson, 1991; Hart *et al.*, 2003; Martin; 1995] (Figure 1a). It was arguably only after this event that the deep-sea sedimentary carbonate system could have 'matured' sufficiently to give rise to the modern mode of marine carbonate cycling and a Cretan ocean [Zeebe and Westbroek, 2003].

This supposition is supported by the composition of Phanerozoic ophiolite suites which indicates that pelagic carbonate accumulation was comparatively rare in Paleozoic deep sea sediments [Boss and Wilkinson, 1991] (Figure 1b). Concurrently, the area of cratonic carbonate accumulation (Figure 1c) is notably diminished during the Mesozoic and Cenozoic as compared to the Paleozoic [Walker *et al.*, 2002], even when contrasting times of similar sea-level. Additional support comes from the restricted presence of epicontinental chalk in pre-Mesozoic high-stand sequences [Boss and Wilkinson, 1991]. The impact of this ecological/evolutionary event is tested by assuming that a present-day potential rate of planktic carbonate production in the open ocean was attained during the Mesozoic – I take the Triassic-Jurassic boundary as the transition point.

The composite model behavior demonstrates a profound change in the regulation of ocean saturation state (Figure 6a). Prior to a 200 Myr interval of saturation stability when surface Ω_{calcite} deviated no more than ± 0.4 from modern, surface saturation during the earlier Phanerozoic undergoes substantial oscillation between the limits $5.8 \leq \Omega_{\text{calcite}} \leq 10.7$. Closely related to this is the depth of the calcite saturation horizon (CSH) (Figure 6b), which exhibits a pronounced excursion during the Permian and Triassic when it lies below 6000 m, with the abyssal ocean bathed in over-saturated conditions. There is some proxy evidence with which to validate the more recent portion of the predicted CSH depth – reconstructions of the average ocean calcite compensation depth (CCD) through the late Mesozoic and Cenozoic [van Andel, 1975; Tyrrell and Zeebe, 2004] (Figure 6b). (The CCD is defined as the depth at which the rain flux of calcite to the sediments exactly balances the dissolution flux back to the ocean, and operationally delineated by the boundary in depth between sediments that have carbonate present and those in which it is completely absent [Berger and Winterer, 1974].) That the predicted CSH

depth parallels that of the reconstructed CCD is certainly encouraging. A chance match cannot be ruled out, however, because the CCD need not *a priori* have a fixed relationship with the depth of the CSH [Sigman *et al.*, 1998].

In contrast to ocean saturation, the evolution of pH exhibits much less of a change in behavior when switching between the Neritan and Cretan ocean modes and during the earlier part of the Phanerozoic is only some ~ 0.05 pH units higher than it would have been in the absence of a deep-sea sedimentary sink. Thus, overall, ocean pH is responding primarily to changes in atmospheric $p\text{CO}_2$ and oceanic $[\text{Ca}^{2+}]$.

Ocean surface pH over the past 60 Myr exhibits an increasing trend which is consistent with paleo-acidity $\delta^{11}\text{B}$ proxy reconstructions, but only in as much as both suggest that the ocean was more acidic at the beginning of the Cenozoic compared to at the end [Pearson and Palmer, 2000] (Figure 6c). The model predicted increase in pH over this interval is only about 50% of the ca. 0.8 pH unit change deduced by Pearson and Palmer [2000]. Although one would not normally question data over model predictions, the residence time of Boron in the ocean is much shorter (20 Myr) than the 60 Myr time frame considered, which could invalidate the underlying assumption that the $\delta^{11}\text{B}$ composition of the ocean is invariant. Indeed, analysis of the marine boron isotope budget suggests that foraminiferal $\delta^{11}\text{B}$ records may in part reflect changes in the marine boron isotope budget rather than changes in ocean pH over the Cenozoic Era, and variation of seawater pH may not have been as important on this time scale [Lemarchand *et al.*, 2000, 2002]. There is also a close agreement between the predictions of this study, which for pH and saturation state are in effect inverse modeled from atmospheric CO_2 and $[\text{Ca}^{2+}]$, and that of Tyrrell and Zeebe [2004] where they take a different analytical approach and directly assimilate

the depth of the CCD (which is equivalent to assuming saturation state is known). The *pH* increase over the last 60 Ma predicted by both model approaches is very similar (~ 0.4 *pH* units).

4. Discussion – A Mid Mesozoic Revolution in global carbon cycling?

With the proliferation of calcareous plankton, the Mesozoic saw a revolution in how ocean chemistry and the global carbon cycle are stabilized. Prior to this time, secular oscillation in sea-level and the extent of epeiric seas, in weathering rates, and in oceanic calcium ion concentrations all drove perturbations of carbonate deposition and ocean chemistry that could only be weakly buffered. This is nowhere more apparent than in the variability of surface saturation state which exhibits an extreme excursion around the time of the Permian and Triassic when ocean surface saturation exceeding $\Omega_{\text{calcite}} = 9$ (Figure 6a). This is a sufficient degree of over-saturation for the development of carbonate crusts and tufas [*Merz-Preiss and Riding, 1999*], particularly in the warmer surface regions of the ocean box model which exceed the mean ocean value presented in the Figures by $\Delta\Omega_{\text{calcite}} \geq 1.0$. Overturn of an anoxic ocean need not necessarily then be invoked in order to account for observations of ‘anomalous’ Permian precipitates [*Grotzinger and Knoll, 1995*]. Instead, in the absence of a deep-sea sedimentary sink the occurrence of a low sea-level stand and associated restriction of carbonate deposition to relatively narrow continental shelves is a sufficient condition in itself. The relatively high oceanic $\text{Mg}^{2+}/\text{Ca}^{2+}$ ratio at this time [*Horita et al., 2002; Lowenstein et al., 2001, 2003*] would enhance the sea-level effect by inhibiting calcite precipitation [*Davis et al., 2000*] until even higher levels of over-saturation are attained.

The late Precambrian is characterized by the widespread occurrence of abundant environmentally controlled carbonates such as cements, calcified cyanobacteria, and thick precipitated beds [Grotzinger and Knoll, 1995; Riding, 1993; Sumner and Grotzinger, 1996]. Similarly low sea-level (and high Mg^{2+}/Ca^{2+}) conditions also prevailed, suggestive of the same causative link as for the Permian/Triassic. Even without additional enhancement of saturation state in the absence of biologically-driven precipitation of carbonate, mean surface Ω_{calcite} exceeds 9 (Figure 6a).

The late Cenozoic sees a third occurrence of low sea-level (Figure 3). Yet we do not see a similar widespread occurrence of abundant environmentally controlled carbonates in the modern marine environment. Why? Although not explicitly tested it was suspected that the reason for this lay in the mode change in carbonate deposition and shift in locus of deposition that was heralded by the Mesozoic proliferation of calcareous plankton [Riding, 1993; Sumner and Grotzinger, 1996]. The model results presented here confirm the plausibility of this explanation and show that the introduction of a deep-sea carbonate buffer led to the regulation of ocean saturation to within ± 0.4 over the subsequent 200 Myr (Figure 6a).

In addition to increased stability, the development of a deep-sea sedimentary sink also results in a lowering of the baseline saturation state of the ocean. This is manifested in lower Cretaceous Ω compared to the Ordovician-through-Devonian (Figure 6a); all times of similarly high sea-level. This is consistent with the observed decline in the abundance of reefal microbialite and absence of calcimicrobe and biocementstone reef frameworks after the Triassic [Webb, 1996]. Again, the Mid Mesozoic Revolution represents a marked transition point in Phanerozoic carbon cycling and ocean chemistry.

One should note that a sharp (instantaneous) transition between Neritan and Cretan oceans has been prescribed here. The development of a substantive deep-sea sedimentary carbonate sink could well have taken place over many tens of millions of years. Unfortunately, compendiums of ophiolite suite composition do not resolve the details of the transition [*Boss and Wilkinson, 1991*]. However, that the last occurrence of abundant environmentally controlled carbonates and biocementstones was during the late Triassic [*Riding, 1993; Webb, 1996*] is consistent with a substantive deep-sea sedimentary carbonate sink developing only after this time. Exactly when during the Jurassic (or later) and how quickly is more of an open question.

Recognizing the role of changes in the mode of carbonate deposition in affecting ocean carbonate chemistry enables new estimates for several key metrics of the Phanerozoic Earth system to be made. I consider three case studies in which assumptions made regarding prevailing marine geochemistry are critical to the overall conclusions; paleo- $p\text{CO}_2$ estimation from carbonate $\delta^{11}\text{B}$ (typically requiring estimates of DIC or ALK), mass-balance interpretation of carbonate $\delta^{13}\text{C}$ excursions (requiring DIC and atmospheric CO_2 inventory), and $p\text{H}$ -correction of paleo-temperature estimates derived from carbonate $\delta^{18}\text{O}$.

4.1 Paleo- $p\text{CO}_2$ estimation from Boron isotopes

The relative incorporation (fractionation) between the two naturally occurring stable isotopes of Boron in precipitating carbonate is $p\text{H}$ -dependent [*Hemming and Hanson, 1991; Palmer and Swihart, 1996*]. This allows, in theory at least, measurements made of carbonate $\delta^{11}\text{B}$ to be interpreted directly in terms of the paleo- $p\text{H}$ of the marine environment. An early application was in reconstructing changes in $p\text{H}$ for late Pleistocene glacial and interglacial periods [*Sanyal et al., 1995, 1997*]. Because ocean DIC and ALK during the last glacial could not have deviated

greatly from modern, it is relatively straightforward to estimate CO₂ partial pressures [Sanyal *et al.*, 1995, 1997]. The δ¹¹B paleo-pH proxy has more recently been applied to estimating *p*CO₂ during the Cenozoic in general [Pearson and Palmer, 1999a, 2000]. The problem as one goes back further in time is in estimating the value of a second property of the aqueous carbonate system. Constant DIC was assumed by Pearson and Palmer [1999a] in their reconstruction of Middle Eocene *p*CO₂, but was subsequently challenged [Caldeira and Berner, 1999]. An alternative suggestion of constant carbonate ion concentration [Caldeira and Berner, 1999] is also questionable [Pearson and Palmer, 1999b]. In reconstructing *p*CO₂ from 60 Ma to present Pearson and Palmer [2000] therefore attempted to assimilate additional information by assuming that the saturation state of the ocean conformed to observed changes in the CCD [van Andel, 1975] and that a direct proportionality existed between changes in ALK and [Ca²⁺]. From this they deduced a decline in ALK from ~4000 μmol eq. kg⁻¹ at 60 Ma to ~2000 μmol eq. kg⁻¹ at 30 Ma and in the range 2000-2400 μmol eq. kg⁻¹ thereafter [Pearson and Palmer, 2000].

Because atmospheric CO₂ and ocean [Ca²⁺] are the primary controls on bulk ocean chemistry and exert antagonistic influences their effects can potentially cancel out. I predict such an occurrence during the last 100 Myr when both CO₂ and Ca²⁺ exhibit strongly decreasing trends (Figure 3). The result is relatively little variability in DIC and ALK, consistent with the analysis of Tyrrell and Zeebe [2004]. The model results presented here thus support the earlier assumption of Pearson and Palmer [1999a] of near modern DIC for the Middle Eocene but do not support elevated ALK during the early Cenozoic [Pearson and Palmer, 2000]. As demonstrated by Tyrrell and Zeebe [2004], the consequence of assuming ca. 2000 μmol eq. kg⁻¹ ALK is a reconstructed *p*CO₂ value of ~1000 μatm for the early Cenozoic rather than the 2000-3000 μatm deduced by Pearson and Palmer [2000] on the basis of ca. 4000 μmol eq. kg⁻¹. This

degree of sensitivity of $p\text{CO}_2$ to alkalinity assumptions demonstrates the importance of making mechanistic model estimations of past ocean chemistry.

4.2 Interpretation of $\delta^{13}\text{C}$ excursions

The magnitude of the ocean DIC inventory has important implications for the interpretation of carbon isotopic ($\delta^{13}\text{C}$) excursions observed in the geologic record such as explained by the release to the ocean (and/or atmosphere) of a source of relatively ^{13}C -depleted carbon. The mechanism invoked is frequently that of the destabilization of methane (CH_4) clathrates [Dickens *et al.*, 1995; Jiang *et al.*, 2003; Kennedy *et al.*, 2001], although oxidation of dissolved organic matter in the ocean has been suggested as critical during the late Precambrian [Rothman *et al.*, 2003]. Mass balance calculation of the quantity of clathrate carbon consistent with the magnitude of the $\delta^{13}\text{C}$ excursion requires knowledge of the ocean carbon inventory. (Strictly the combined ocean + atmosphere + biosphere inventory, although the ocean dominates the total inventory over the range of possible Phanerozoic atmospheric CO_2). The model prediction of Phanerozoic ocean chemistry made here has bearing on this.

For instance, the mass of isotopically light carbon required to reproduce the ca. -2.5 $\delta^{13}\text{C}$ excursion recorded at the Paleocene-Eocene boundary at 55.5 Ma [Bains *et al.*, 1999; Dickens *et al.*, 1995] can be calculated on the basis of a near-modern ocean carbon inventory (Figure 6d). Some 1.6×10^{18} g of methane carbon is required assuming a $\delta^{13}\text{C}$ for clathrate methane of -60‰. In contrast, explanations for the excursions marking the end of the Permian at 251 Ma will require a carbon perturbation more than twice as large per mil of excursion because mean ocean DIC exceeds $5000 \mu\text{mol kg}^{-1}$ at this time. For a 2-4‰ negative excursion in $\delta^{13}\text{C}$ [Payne *et al.*, 2004], between 3.0×10^{18} and 6.0×10^{18} gC would be required. While substantial, the required

quantity of clathrate to be destabilized is still less than the consensus estimate of 1.0×10^{19} gC for the modern methane hydrate reservoir [Kvenvolden, 2002].

Going further back in time still, the immediate aftermath of the extreme glaciations of the late Neoproterozoic were marked by isotopic excursions recorded in the post glacial ‘cap’ carbonate facies of -4 to -7‰ [Hoffman *et al.*, 1998; Jacobsen and Kaufman, 1999; Kennedy *et al.*, 1998]. The cause of these changes has also been proposed to be the destabilization of methane clathrates [Jiang *et al.*, 2003; Kennedy *et al.*, 2001]. If modern ocean chemistry is assumed in the calculation [Jiang *et al.*, 2003; Kennedy *et al.*, 2001] only between 2.6 and 4.7×10^{18} gC is required to explain the excursion. In contrast, the model prediction made here indicates that the late Precambrian had an exchangeable (ocean+atmosphere) carbon reservoir over 4 times modern (Figure 6d). The required release of clathrate carbon is then between 1.1×10^{19} g and 1.9×10^{19} g, which exceeds all but the most extreme estimates for the modern hydrate inventory [Kvenvolden, 2002].

4.3 Ocean pH and the reconstruction of paleo-temperature

What controls the onset of ice ages and ‘cool’ intervals during the Phanerozoic (Figure 7a)? Several recent studies have addressed this question [Royer *et al.*, 2004; Shaviv and Veizer, 2004; Veizer *et al.*, 2000] but come to very different conclusions. The point of contention is whether reconstructed anomalies in Phanerozoic climate best correlate with the concentration of CO₂ in the atmosphere (either proxy-derived or model-predicted) [Royer *et al.*, 2004], or whether a better correlation is found with some more exotic driver of climate such as cosmic ray flux [Shaviv, 2002; Shaviv and Veizer, 2003]. However, in order to successfully chose between these competing hypotheses for the driver of Phanerozoic climate change one must *a priori* have

confidence that the record of climate anomalies has been reconstructed with some fidelity and that the wiggles in the curve really are significant. I do not believe that this to be the case.

Although proxies for paleo sea-ice limits and tillite occurrence can provide important first-order constraints on the past extent of continental glaciation (Figure 7a), a more quantitative reconstruction has been proposed based on the oxygen isotopic composition ($\delta^{18}\text{O}$) of well-preserved carbonates [Veizer *et al.*, 1999, 2000] (Figure 7b). This involves first removing a linear $\sim 8\text{‰}$ trend from this data-set to create a $\delta^{18}\text{O}$ residual [Veizer *et al.*, 2000]. This residual is then interpreted as a proxy for anomalies in tropical SSTs. The result is an apparent secular oscillation in climate, with ‘cool’ modes centered around the Ordovician-Silurian, Carboniferous-Permian, and Jurassic-Cretaceous boundaries, and during the Neogene, and ‘warm’ modes prior to the mid Ordovician, during the Devonian, the late Permian and Triassic, and late Cretaceous (Figure 7c) [Veizer *et al.*, 2000; Shaviv and Veizer, 2003].

Building on earlier work by Zeebe [1999], Royer *et al.* [2004] recognized that in addition to reflecting the isotopic composition and temperature of the precipitating solution, $\delta^{18}\text{O}$ recorded in carbonates should also be a function of ambient pH [Spero *et al.*, 1997; Bemis *et al.*, 1998; Zeebe, 1999]. Any change in surface ocean pH will affect the $\delta^{18}\text{O}$ signature of precipitated carbonates and generate a ‘phantom’ climate signal over-printed onto that due to the ‘real’ ΔT variability. Royer *et al.* [2004] made an estimate of Phanerozoic ocean pH to correct the ΔT record of Veizer *et al.* [2000] for this effect and found that the reconstructed ΔT curve (Figure 7c) no longer correlated well with the Shaviv [2002] cosmic ray flux reconstruction. Instead it bore a close relationship to $p\text{CO}_2$ (Figure 7c), interpreted as supporting the role of CO_2 as a primary driver of Phanerozoic climate.

I re-visit this argument by utilizing the oceanic pH curve predicted using the mechanistic atmosphere-ocean-sediment carbon cycle model predictions, and apply the same pH - $\delta^{18}\text{O}$ and $\delta^{18}\text{O}$ - ΔT relationships as *Royer et al.* [2004] (i.e., *Zeebe* [2001]) to re-calculate ΔT from the linearly detrended $\delta^{18}\text{O}$ data of *Veizer et al.* [2000]. The results of this are consistent with *Royer et al.* [2004] (compare Figure 8a with Figure 7c). However, I believe that the manner in which the $\delta^{18}\text{O}$ curve has been corrected to obtain this result is flawed. The reasoning is as follows. The existence of a secular trend in pH implies that pH -dependent ^{18}O fractionation contributes to the underlying trend in the carbonate $\delta^{18}\text{O}$ time-series. The linear component of the predicted oceanic pH variability since 500 Ma (Figure 6c) is 0.58 pH units, equivalent to a change in $\delta^{18}\text{O}$ of -0.82‰. By fully de-trending the raw $\delta^{18}\text{O}$ data, the linear -0.82‰ contribution made by pH has already been implicitly removed. Thus, if a pH correction is to be applied to the de-trended $\delta^{18}\text{O}$, the pH signal must first be linearly de-trended itself.

The result of carrying out a linear de-trending of the reconstructed pH data (slope $\Delta pH = -0.00115t$, where t is the age in Ma) before applying the pH - $\delta^{18}\text{O}$ and $\delta^{18}\text{O}$ - ΔT correlations to the ‘residual’ $\delta^{18}\text{O}$ of *Veizer et al.* [2000] is shown in Figure 8b. The signal now lacks the Mid and Early Paleozoic elevated ΔT of *Royer et al.* [2004] which I believe to be an artifact caused by removing the linear component due to pH twice. However, neither is there much support for the prominent Ordovician/Silurian ‘cool’ mode of *Shaviv and Veizer* [2003]. In addition, all of the Cretaceous remains as a prominent ‘warm’ mode.

One must recognize that the zero line lays within the ΔT uncertainty limits for more than half of the 430 Myr interval analyzed. Because of a lack of proxy CO_2 data before this no uncertainty limits can be calculated for the Ordovician/Silurian. However, applying an

appropriate degree of uncertainty, say $\pm 1.5^{\circ}\text{C}$, one would conclude that global climate during the Ordovician/Silurian was not distinguishable from the baseline. Furthermore, the plotted uncertainty limits are those arising solely from 1 standard deviation of the proxy atmospheric CO₂ data. The additional uncertainty due to reconstructed [Ca²⁺] – equivalent to about $\pm 0.1 \text{ pH}$ units or $\pm 0.6^{\circ}\text{C}$ in ΔT , would then further push the zero line within uncertainty for all but three main periods – the Cretaceous (warm anomaly), Carboniferous (cold anomaly), and late Cambrian (warm anomaly).

4.4 Caveats and future work

There are important limitations to this modeling exercise, of course, particularly in terms of the restricted spatial resolution of the ocean circulation model used. In addition, without a coupled climate model the effect of changes in global temperature on the latitudinal limits of reefal carbonate production cannot be accounted for. Because of this, little can be said about the spatial distribution of cratonic carbonate accumulation and validation of the model cannot easily be made against available geologic reconstructions of this [Kiessling *et al.*, 2003; Mackenzie and Morse, 1992; Walker *et al.*, 2002]. Work underway will address this through the use of a more spatially resolved Earth system model ('genie'; www.genie.ac.uk). By specifying appropriate continental configurations for each time-slice, a self-consistent set of ocean circulation and global climatic states will provide the necessary physical boundary conditions for the marine carbonate cycle. This will allow the degree of continental fragmentation as well as paleo-latitude to be taken into account in the calculation of weathering fluxes (e.g., Donnadieu *et al.* [2004], Gibbs *et al.* [1999]). An Earth system model with explicit 2D spatial resolution will also allow improvements to be made in the neritic carbonate depositional model. For instance, a mechanistic sedimentological model (e.g., Burgess, 2001) could be combined with a mechanistic

representation of coral growth and carbonate production (e.g., *Kleypas*, 1997). Obviously there would be a computational penalty to this, which highlights the value of carrying out exploratory studies with the aid of a much less highly resolved and more efficient model first.

5. Conclusions

The Phanerozoic has seen dramatic changes in ocean chemistry and carbonate cycling with implications for the interpretation of the geological record and of paleo climate proxies. I find a secular trend in ocean pH over the Phanerozoic of ~0.6 pH units, the presence of which must be recognized if carbonate $\delta^{18}\text{O}$ ‘residuals’ are to be interpreted in terms of surface temperature anomalies. However, the range of uncertainty inherent in estimates of paleo CO₂ alone leaves some of the previously-identified $\delta^{18}\text{O}$ -derived temperature ‘anomalies’ indistinguishable from zero, with just the Cretaceous (warm anomaly), Carboniferous (cold anomaly), and late Cambrian (warm anomaly) significant.

Dissolved inorganic carbon and alkalinity concentrations changed little over the last 100 Myr. Inventories are substantially enhanced earlier than this however; 2- to 3-fold during the early-to-mid Mesozoic, 3-fold during the early-to-mid Paleozoic, and more than 4-fold in the late Precambrian. This variability must be taken into account in the interpretation $\delta^{13}\text{C}$ excursions. Previous studies of Neoproterozoic excursions may have very substantially underestimated the quantity of clathrate carbon required to explain them.

Overall, the Mid Mesozoic saw a revolution in how the global carbon cycle was stabilized with the proliferation of planktic calcifiers representing a profound change in the biogeochemical cycling of calcium carbonate. Prior to this time extreme excursions in ocean saturation state

would have occurred during periods of low sea-level such as the Permian and late Precambrian, which helps explain the often ‘anomalous’ character of precipitated carbonates during these times. The Mid Mesozoic Revolution heralded the development of a responsive deep-sea carbonate sink that introduced a new and powerful negative feedback to the Earth system. The relatively low degree of over-saturation of the modern ocean and absence of environmentally controlled carbonates is a direct and predictable consequence of this.

AJR acknowledges support for this work from Canada Research Chairs and the Trusthouse Charitable Foundation. I am grateful to the two reviewers for their in-depth, constructive, and at times, light-hearted comments on the manuscript.

References

- Algeo, T. J., K. B. Sleslavinsky, The paleozoic world - Continental flooding, hypsometry, and sealevel, *American Journal of Science*, **295**, 787-822, 1995.
- Archer, D., An atlas of the distribution of calcium carbonate in sediments of the deep sea, *Global Biogeochemical Cycles*, **10**, 159-174, 1996a.
- Archer, D., A data-driven model of the global calcite lysocline, *Global Biogeochemical Cycles*, **10**, 511-526, 1996b.
- Archer, D., A. Winguth, D. Lea, and N. Mahowald, What caused the glacial/interglacial atmospheric $p\text{CO}_2$ cycles?, *Reviews of Geophysics*, **38**, 159-189, 2000.
- Archer, D., Who Threw That Snowball?, *Science*, **302**, 791-780, 2003.

Arp, G., V. *et al.*, Biofilm exopolymers control microbialite formation at thermal springs discharging into the alkaline Pyramid Lake, Nevada, USA, *Sedimentary Geology*, **126**, 159-176, 1999.

Bains, S., R. M. Corfield, and R. D. Norris, Mechanisms of climate warming at the end of the Paleocene, *Science*, **285**, 724-727, 1999.

Bemis, B. E., *et al.*, Reevaluation of the oxygen isotopic composition of planktonic foraminifera: Experimental results and revised paleotemperature equations, *Paleoceanography*, **13**, 150-160, 1998.

Berger, W. H., and E. L. Winterer, Plate stratigraphy and the fluctuating carbonate line, in In Hsü, K. J., and H. C. Jenkins (eds.), Pelagic Sediments: on Land and under the Sea, Special Publication no. 1, International Association of Sedimentologists, 1974.

Berner, R. A., Atmospheric carbon dioxide levels over Phanerozoic time, *Science*, **249**, 1382-1386, 1990.

Berner, R. A., Weathering, plants, and the long-term carbon cycle, *Geochimica et Cosmochimica Acta*, **56**, 3225-3231, 1992.

Berner, R. A., 3Geocarb II: A revised model of atmospheric CO₂ over Phanerozoic time, *American Journal of Science*, **294**, 56-91, 1994.

Berner, R. A., and K. Caldeira, The need for mass balance and feedback in the geochemical carbon cycle, *Geology*, **25**, 955-956, 1997.

Berner, R. A., and Z. Kothavala, GEOCARB III: A revised model of atmospheric CO₂ over Phanerozoic time, *American Journal of Science*, **301**, 182-204, 2001.

Boss, S. K., B. H. Wilkinson, Planktogenic eustatic control on cratonic oceanic carbonate accumulation, *Journal of Geology*, **99**, 497-513, 1991.

Broecker, W. S., and T-H. Peng, Glacial to interglacial changes in the operation of the global carbon cycle, *Radiocarbon*, **28**, 309-327, 1986.

Burgess, P. M., Modeling carbonate sequence development without relative sea-level oscillations, *Geology*, **29**, 1127-1130, 2001.

Burton, E. A., L. M. Walter, Relative precipitation rates of aragonite and mg calcite from seawater - Temperature or carbonate ion control, *Geology*, **15**, 111-114, 1987.

Caldeira, K., and R. Berner, Seawater pH and Atmospheric Carbon Dioxide, *Science*, **286**, 2043a, 1999.

Caldeira, K., M. R. Rampino, Aftermath of the end-cretaceous mass extinction - possible biogeochemical stabilization of the carbon-cycle and climate, *Paleoceanography*, **8**, 515-525, 1993.

Crowell, J. C., Pre-Mesozoic Ice Ages: Their Bearing on Under-standing the Climate System, Mem. Geol. Soc. Am., 192, 1999.

Crowley, T. J., Significance of tectonic boundary conditions for paleoclimate simulations, in: Crowley, T. J. and K. C. Burke (Eds.), *Tectonic Boundary Conditions for Climate Reconstructions*, Oxford University Press, p. 3-17, 1998.

Davis, K. J., *et al.*, The role of Mg²⁺ as an impurity in calcite growth, *Science*, **290**, 1134-1137, 2000.

Dickens, G. R., *et al.*, Dissociation of oceanic methane hydrate as a cause of the carbon-isotope excursion at the end of the Paleocene, *Paleoceanography*, **10**, 965-971, 1995.

Dickson, J. A. D., Fossil echinoderms as monitor of the Mg/Ca ratio of phanerozoic oceans, *Science*, **298**, 1222-1224, 2002.

Donnadieu, Y., *et al.*, A ‘snowball Earth’ climate triggered by continental break-up through changes in runoff, *Nature*, **428**, 303-306, 2004.

Frakes, L. A., *et al.*, 1992, Climate modes of the Phanerozoic; The history of the Earth’s climate over the past 600 million years: Cambridge, Cambridge University Press, 286 p., 1992.

Franck, S., *et al.*, Modelling the global carbon cycle for the past and future evolution of the earth system, *Chemical Geology*, **159**, 305-317, 1999.

Franck, S., *et al.*, Reduction of biosphere life span as a consequence of geodynamics, *Tellus B*, **52**, 94-107, 2000.

Gibbs, M. T., *et al.*, Global chemical erosion over the last 250 my: Variations due to changes in paleogeography, paleoclimate, and paleogeology, *American Journal of Science*, **299**, 611-651, 1999.

Grotzinger, J. P., and A. H. Knoll, Anomalous carbonate precipitates: Is the precambrian the key to the Permian?, *Palaios*, **10**, 578-596, 1995.

Haq, B.U., *et al.*, Mesozoic and Cenozoic chronostratigraphy and cycles of sea-level change, in Wilgus, C. K., *et al.*, (eds.), Sealevel-changes; an integrated approach: Society of Economic Paleontologists and Mineralogists, Special Publication, 42, 71-108, 1988.

Hallam, A., Pre-Quaternary sea-level changes, *Annual Review of Earth and Planetary Sciences*, **12**, 205-243, 1984.

Hargreaves, J. C., J. D. Annan, N. R. Edwards and R. Marsh, Climate forecasting using an intermediate complexity Earth system model and the Ensemble Kalman Filter. *Climate Dynamics*, in press.

Hart, M. B., *et al.*, The search for the origin of the planktic Foraminifera, *Journal of the Geological Society*, **160**, 341-343, 2003.

Hemming, N. G., and G. N. Hanson, Boron isotopic composition and concentration in modern marine carbonates, *Geochimica et Cosmochimica Acta*, **56**, 537-543, 1991.

Horita, J., *et al.*, Chemical evolution of seawater during the Phanerozoic: Implications from the record of marine evaporates, *Geochimica et Cosmochimica Acta*, **66**, 3733-3756, 2002.

Jacobsen, S. B., A. J. Kaufman, The Sr, C and O isotopic evolution of Neoproterozoic seawater, *Chemical Geology*, **161**, 37-57, 1999.

Jacquin, T., and P. R. Vail, Shelfal accommodation as a major control on carbonate platforms, *Bulletin de la Societe Geologique de France*, **166**, 423-435, 1995.

Jiang, G., *et al.*, Stable isotopic evidence for methane seeps in Neoproterozoic postglacial cap carbonates, *Nature*, **426**, 822-826, 2003.

Kennedy, M. J., B. Runnegar, A. R. Prave, K. H. Hoffmann, M. A. Arthur, Two or four Neoproterozoic glaciations?, *Geology*, **26**, 1059-1063, 1998.

Kennedy, M. J., *et al.*, Are Proterozoic cap carbonates and isotopic excursions a record of gas hydrate destabilization following Earth's coldest intervals?, *Geology*, **29**, 443-446, 2001.

Kiessling, W., E. Flügel, and J. Golonka, Patterns of Phanerozoic carbonate platform sedimentation, *Lethaia*, **36**, DOI: 10.1080/00241160310004648, 2003

Kleypas, J. A., Modeled estimates of global reef habitat and carbonate production since the last glacial maximum, *Paleoceanography*, **12**, 533-545, 1997.

Leclercq, N., J. P. Gattuso, J. Jaubert, CO₂ partial pressure controls the calcification rate of a coral community, *Global Change Biology*, **6**, 329-334, 2000.

Lowenstein, T. K., *et al.*, Oscillations in Phanerozoic seawater chemistry: Evidence from fluid inclusions, *Science*, **294**, 1086-1088, 2002.

Lowenstein, T. K., *et al.*, Secular variation in seawater chemistry and the origin of calcium chloride basinal brines, *Geology*, **31**, 857-860, 2003.

Mackenzie, F. T., and J. W. Morse, Sedimentary carbonates through Phanerozoic time, *Geochimica et Cosmochimica Acta*, **56**, 3281-3295, 1992.

Maier-Reimer, E., Geochemical cycles in an ocean general circulation model. Preindustrial tracer distributions, *Global Biogeochemical Cycles*, **7**, 645-677, 1993.

Marshall, A. T., P. L. Clode, Effect of increased calcium concentration in sea water on calcification and photosynthesis in the scler-actinian coral *Galaxea fascicularis*, *Journal of Experimental Biology*, **205**, 2107-2113, 2002.

Martin, R. E., Cyclic and secular variation in microfossil biomineralization - clues to the biogeochemical evolution of Phanerozoic oceans, *Global and Planetary Change*, **11**, 1-23, 1995.

Merz-Preiss, M., and R. Riding, Cyanobacterial tufa calcification in two freshwater streams: ambient environment, chemical thresholds and biological processes, *Sedimentary Geology*, **126**, 103-124, 1999.

Milliman, J. D., A. W. Droxler, Neritic and pelagic carbonate sedimentation in the marine environment: Ignorance is not bliss, *Geologische Rundschau*, **85**, 496-504, 1996.

Milliman, J. D., *et al.*, Biologically mediated dissolution of calcium carbonate above the chemical lysocline?, *Deep-Sea Research I*, **46**, 1653-1669, 1999.

Morse, J. W., S. L. He, Influences of T, S and $p\text{CO}_2$ on the pseudo-homogeneous precipitation of CaCO_3 from seawater – Implications for whiting formation, *Marine Chemistry*, **41**, 291-297, 1993.

Munhoven, G., Glacial-interglacial changes of continental weathering: estimates of the related CO_2 and HCO_3^- flux variations and their uncertainties, *Global and Planetary Change*, **33**, 155-176, 2002.

Munhoven, G., and L. M. François, Glacial-interglacial variability of atmospheric CO_2 due to changing continental silicate rock weathering: A model study, *Journal of Geophysical Research*, **101**, 21423-21437, 1996.

Opdyke, B. N., and B. H Wilkinson, Carbonate mineral saturation state and cratonic limestone accumulation, *American Journal of Science*, **293**, 217-234, 1993.

Palmer, M. R., and G. H. Swihart, Boron isotope geochemistry: An overview, *Rev. Mineralogy*, **33**, 709-744, 1996.

Payne, J. L., et al., Large perturbations of the carbon cycle during recovery from the end-Permian extinction, *Science*, **305**, 506-509, 2004.

Pearson, P. N., and M. R. Palmer, Middle Eocene seawater pH and atmospheric carbon dioxide concentrations, *Science*, **284**, 1824-1826, 1999a.

Pearson, P. N., and M. R. Palmer, Seawater pH and Atmospheric Carbon Dioxide, *Science*, **286**, 2043a, 1999b.

Pearson, P. N., and M. R. Palmer, Atmospheric carbon dioxide concentrations over the past 60 million years, *Nature*, **406**, 695-699, 2000.

Rahmstorf, S. *et al.*, Cosmic Rays, Carbon Dioxide, and Climate, *EOS*, **85**, 38-41, 2004.

Ridgwell, A. J., Glacial-interglacial perturbations in the global carbon cycle, PhD thesis, Univ. of East Anglia at Norwich, UK, 2001. (http://tracer.env.uea.ac.uk/e114/ridgwell_2001.pdf)

Ridgwell, A. J., A. J. Watson, and D. E. Archer, Modelling the response of the oceanic Si inventory to perturbation, and consequences for atmospheric CO₂, *Global Biogeochemical Cycles*, **16**, 1071, DOI:10.1029/2002GB001877, 2002.

Ridgwell, A. J., *et al.*, Carbonate deposition, climate stability, and Neoproterozoic ice ages, *Science*, **302**, 859-862, 2003.

Ridgwell, A. J., and M. J. Kennedy, Secular changes in the importance of neritic carbonate deposition as a control on the magnitude and stability of Neoproterozoic ice ages, in: *The Extreme Proterozoic: Geology, Geochemistry, and Climate*, Eds. Jenkins, G., et al., Geophysical Monograph Series Volume 146, American Geophysical Union, Washington DC, 2004.

Riding, R., Phanerozoic patterns of marine CaCO₃ precipitation, *Naturwissenschaften*, **80**, 513-516, 1993.

Riebesell, U., I. Zondervan, B. Rost, P. D. Tortell, R. E. Zeebe, F. M. M. Morel, Reduced calcification of marine plankton in response to increased atmospheric CO₂, *Nature*, **407**, 364-367, 2000.

Rothman, D. H., *et al.*, Dynamics of the Neoproterozoic carbon cycle, *Proceedings of the National Academy of Sciences of the United States Of America*, **100**, 8124-8129, 2003.

Royer, D. L., *et al.*, CO₂ as a primary driver of Phanerozoic climate, *GSA Today*, **14**, 4–10, 2004.

Sandberg, P. A., An oscillating trend in Phanerozoic nonskeletal carbonate mineralogy, *Nature*, **305**, 19-22, 1983.

Sanyal, A., *et al.*, Evidence for a higher pH in the glacial ocean from boron isotopes in foraminifera, *Nature*, **373**, 234-236, 1995.

Sanyal, A., *et al.*, Changes in pH in the eastern equatorial Pacific across Stage 5-6 boundary based on boron isotopes in foraminifera, *Global Biogeochemical Cycles*, **11**, 125-133, 1997.

Shaviv, N. J., Cosmic ray diffusion from the galactic spiral arms, iron meteorites, and a possible climatic connection, *Physical Review Letters*, **89**, art. no. 051102, 2002.

Shaviv, N. J., and J. Veizer, Celestial driver of Phanerozoic climate?, *GSA Today*, **13**, 4-10, 2003.

Sigman, D. M., *et al.*, The calcite lysocline as a constraint on glacial/interglacial low-latitude production changes, *Global Biogeochemical Cycles*, **12**, 409-427, 1998.

Spero, H. J., *et al.*, Effect of seawater carbonate concentration on foraminiferal carbon and oxygen isotopes, *Nature*, **390**, 497-500, 1997.

Stanley, S. M., and L. A. Hardie, Secular oscillations in the carbonate mineralogy of reef-building and sediment-producing organisms driven by tectonically forced shifts in seawater chemistry, *Palaeogeography Palaeoclimatology Palaeoecology*, 144, 3-19, 1998.

Stanley, S. M., and L. A. Hardie, Hypercalcification: Paleontology link plate tectonics and geochemistry to sedimentology, *GSA Today*, 9, 1-7, 1999.

Sumner, D. Y., and J. P. Grotzinger, Were kinetics of Archean calcium carbonate precipitation related to oxygen concentration?, *Geology*, 24, 119-122, 1996.

Sundquist, E. T., Influence of deep-sea benthic processes on atmospheric CO₂, *Phil. Trans. R. Soc. Lond. A*, 331, 155-165, 1990.

Sundquist, E. T., Steady-state and non-steady-state carbonate silicate controls on atmospheric CO₂, *Quaternary Science Reviews*, 10, 283-296, 1991.

Tajika, E., Climate change during the last 150 million years: reconstruction from a carbon cycle model, *EPSL*, 160, 695-707, 1998.

Tajika, E., Carbon cycle and climate change during the Cretaceous inferred from a biogeochemical carbon cycle model, *Island Arc*, 8, 293-303, 1999.

Tyrrell, T., and R. E. Zeebe, History of Carbonate Ion Concentration over the last 100 Million Years, *Geochimica et Cosmochimica Acta*, 68, 3521–3530, 2004.

van Andel, T. H., Mesozoic/Cenozoic calcite compensation depth and the global distribution of calcareous sediments, *Earth and Planetary Science Letters*, 26, 187-194, 1975.

Veizer, J., *et al.*, ⁸⁷Sr/⁸⁶Sr, δ¹³C and d¹⁸O evolution of Phanerozoic seawater, *Chemical Geology*, 161, 59-88, 1999.

Veizer, J., et al., Evidence for decoupling of atmospheric CO₂ and global climate during the Phanerozoic eon, *Nature*, **408**, 698-701, 2000.

Walker, L. J., et al., Continental drift and Phanerozoic carbonate accumulation in shallow-shelf and deep-marine settings, *Journal of Geology*, **110**, 75-87, 2002.

Webb, G. E., Was Phanerozoic reef history controlled by the distribution of non-enzymatically secreted reef carbonates (microbial carbonate and biologically induced cement)?, *Sedimentology*, **43**, 947-971, 1996.

Wilkinson, B. H., et al., Submarine hydrothermal weathering, global eustasy, and carbonate polymorphism in Phanerozoic marine oolites, *Journal of Sedimentary Petrology*, **55**, 171-183, 1984.

Wood, R. A., Nutrients, predation and the history of reef-building, *Palaios*, **8**, 526-543, 1993.

Wood, R. A., J. P. Grotzinger, J. A. D. Dickson, Proterozoic modular biomineralized metazoan from the Nama Group, Namibia, *Science*, **296**, 2383-2386, 2002.

Yamanaka, Y., and E. Tajika, The role of the vertical fluxes of particulate organic matter and calcite in the oceanic carbon cycle: Studies using an ocean biogeochemical general circulation model, *Global Biogeochemical Cycles*, **10**, 361-382, 1996.

Zeebe, R. E., An explanation of the effect of seawater carbonate concentration on foraminiferal oxygen isotopes, *Geochimica et Cosmochimica Acta*, **63**, 2001-2007, 1999.

Zeebe, R. E., Seawater pH and isotopic paleotemperatures of Cretaceous oceans, *Palaeogeography Palaeoclimatology Palaeoecology*, **170**, 49-57, 2001.

Zeebe, R. E., and P. Westbroek, A simple model for the CaCO₃ saturation state of the ocean: The “Strangelove,” the “Neritan,” and the “Cretan” Ocean, *Geochem. Geophys. Geosys.* **4**, doi:10.1029/2003GC000538, 2003.

Zeebe, R. E., and D. Wolf-Gladrow, CO₂ in seawater: Equilibrium, kinetics, isotopes, Elsevier Oceanographic Series 65, Elsevier, New York, 2001.

Figure 1. Mode changes in the evolution of global carbonate cycling through the Phanerozoic.

(a) Major changes in plankton assemblages [Martin, 1995]. Calcifying taxa are highlighted in black with non-calcifying taxa shown in grey. The rise during the early- to mid-Mesozoic of the importance of *Globigerinina* is shown as broadly representative of the timing of changes of planktic foraminiferal taxa in general, although the evolution of the first foraminifera taxa occurred somewhat earlier in the mid-Paleozoic [Martin, 1995]. (b) Percent occurrence of carbonates in ophiolite complexes for which sedimentary composition has been reported [Boss and Wilkinson, 1991]. The comparative rarity of carbonate sediments in ophiolite complexes of Paleozoic age is notable. (c) Reconstructed changes in the total area of platform (shallow water) carbonates [Walker *et al.*, 2002].

Figure 2. Schematic of the global carbonate cycle model. (a) The physical structure of the ‘PANDORA’ [Broecker and Peng, 1986] ocean biogeochemical box model which forms the basis of the overall model used in this study. The global ocean is divided into Atlantic, Southern Ocean, and Indo-Pacific basins with up to three vertically-separated water masses. The general form of the prescribed ocean circulation is highlighted in the left-hand side of the diagram. On the right is illustrated the relationship between ocean structure and deep-sea sediment model as well as to weathering input and carbonate removal through neritic deposition. (b) Predicted modern depth distribution of sediment composition (wt% CaCO₃) associated with each oceanographic region. The 0-100% range of wt% CaCO₃ is scaled to the drawn width of each region, and to avoid clutter only the scale axis associated with the low latitude Indo-Pacific region is labeled. The PANDORA model is implemented by transforming onto a 8 × 3 (column × rows) box array which is delineated by the grid of dotted lines. Ocean circulation and biogeochemistry related to the cycling of organic matter in the ocean are essentially identical to that of PANDORA, however.

Figure 3. Prescribed changes in boundary conditions in the model ('forcings'). (a) Phanerozoic evolution of atmospheric CO₂ reconstructed from proxy records [Royer *et al.*, 2004]. Paleo CO₂ data has been binned into 20 Myr intervals, with one standard deviation of the error shown as a vertical black line for each point (filled squares). The raw proxy data is plotted as open circles. Where lack of proxy data requires substitution of values by GEOCARB [Berner and Kothavala, 2001, Royer *et al.*, 2004], points are plotted as filled triangles. (b) Eustatic sea-level plotted relative to modern [Haq *et al.*, 1988]. (c) Model-predicted changes in ocean [Ca²⁺] [Stanley and Hardie, 1998] (solid line) and the fluid inclusion analysis [Horita *et al.*, 2002] (vertical grey bars). (d) Reconstructed changes in the bicarbonate (HCO₃⁻) flux to the oceans due to rock (silicate plus carbonate) weathering through the Cenozoic and Mesozoic [Gibbs *et al.*, 1999]. The solid curve reflects the mean predicted change in weathering rates while the dotted lines represent the maximum and minimum estimates of Gibbs *et al.* [1999] across the different assumptions made regarding paleo atmospheric CO₂ value and temperature dependence of weathering rate.

Figure 4. Response of a Cretan ocean. (a) Mean (area-weighted) surface saturation state with respect to calcite (Ω_{calcite}). The shaded band represents the uncertainty in Ω_{calcite} due to the uncertainty in weathering input (Figure 3d). The horizontal dotted line indicates the simulated present-day value. (b) Mean surface pH. The shaded band represents the uncertainty in pH due to the uncertainty in prescribed atmospheric CO₂ (Figure 3a). The horizontal dotted line indicates the simulated present-day value. (c) Total (solid line) and neritic (dotted) rates of carbonate accumulation. The shaded band represents the uncertainty in accumulation rate due to the uncertainty in weathering input. Before 230 Ma a modern weathering flux is assumed for which no error limits have been calculated.

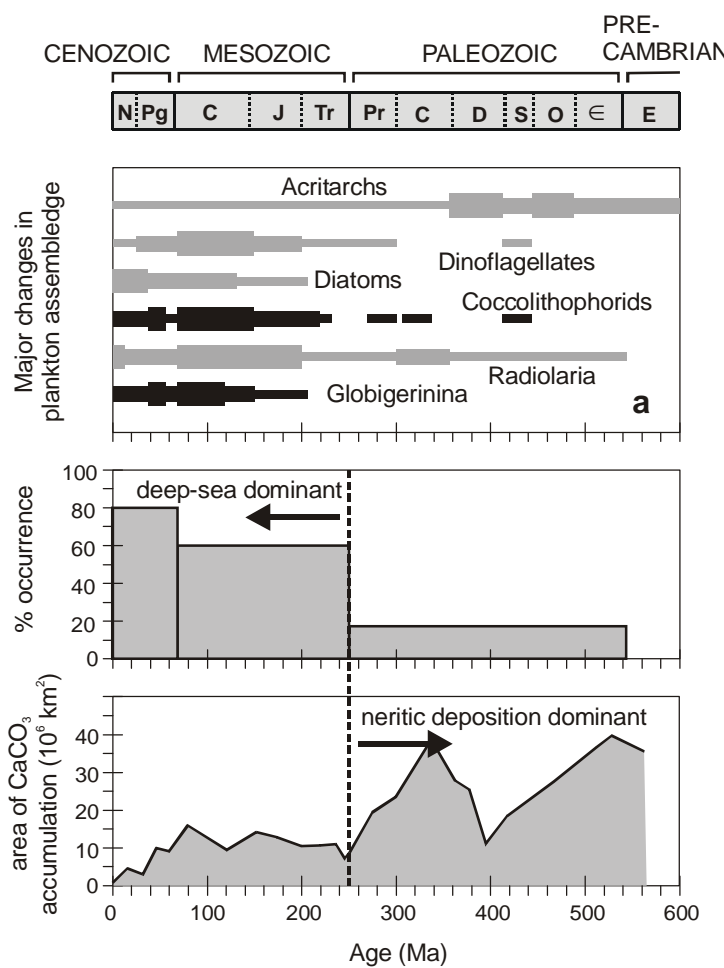
Figure 5. Response of a Neritan ocean. (a) Mean Ω_{calcite} . (b) Mean surface pH. (c) Total (solid line) and neritic (dotted) rates of carbonate accumulation. Now the horizontal lines represent the value predicted for present-day boundary conditions in a Neritan ocean.

Figure 6. Evolution of marine carbonate cycling assuming a transition between Neritan and Cretan ocean modes at 200 Ma. (a) Mean surface saturation state with respect to calcite (Ω_{calcite}). (b) Depth in the ocean of the calcite saturation horizon (solid black line). Plotted for comparison are reconstructions of the evolution of the calcite CCD in the ocean; a composite for the last 100 Myr [Tyrrell and Zeebe, 2004] (thick grey line) and late Mesozoic changes following *Van Andel* [1975] (grey dots). (c) Mean surface pH (solid black line). The Cenozoic trend in surface ocean pH estimated from analysis of foraminiferal carbonate $\delta^{11}\text{B}$ [Pearson and Palmer, 2000] is shown in dark grey. (d) Mean ocean (volume weighted) dissolved inorganic carbon (DIC) concentration. In all the panels the shaded band represents the difference between Cretan and Neritan ocean responses (the uncertainty due to CO_2 and/or weathering is not shown). Horizontal dotted lines indicate simulated present-day values. Also indicated (vertical dotted line) is the prescribed timing of the Mid Mesozoic Revolution (MMR).

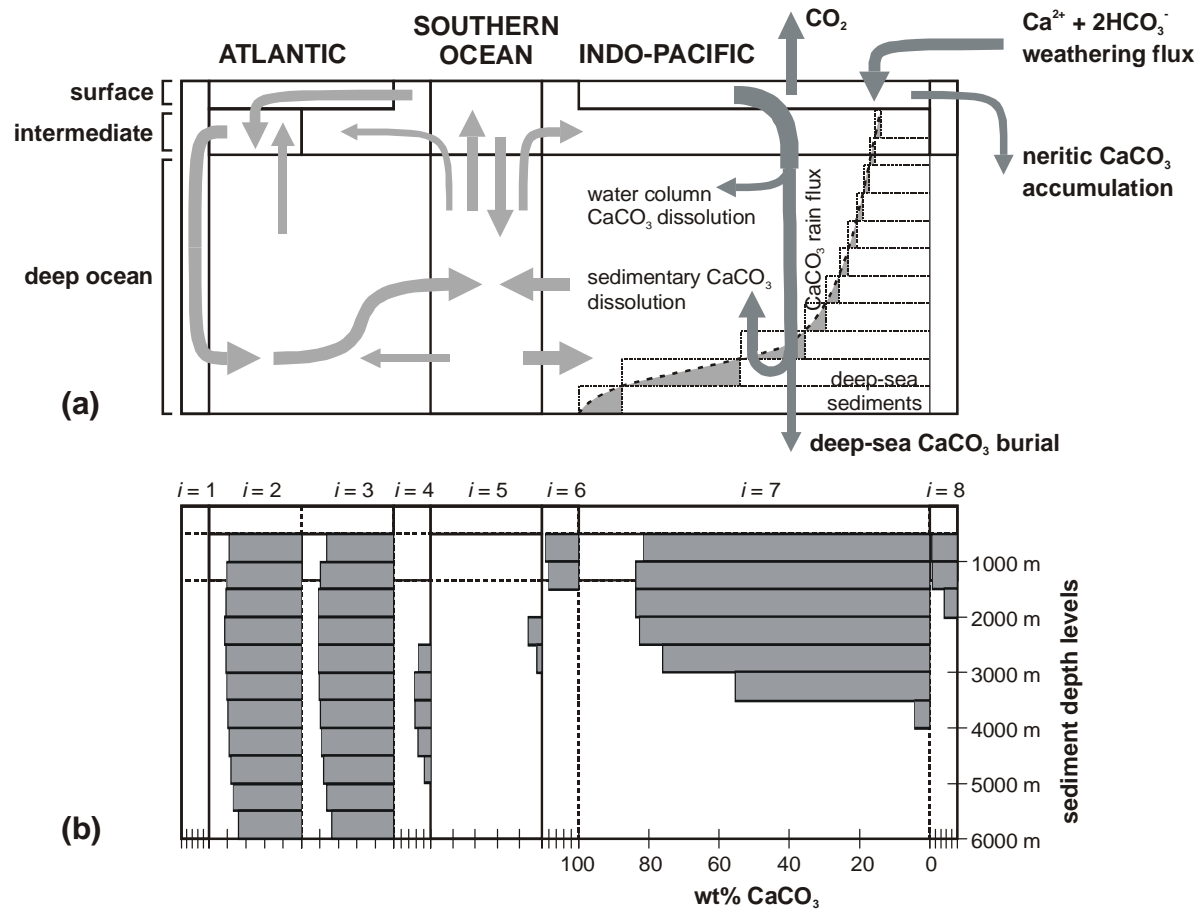
Figure 7. Phanerozoic climate change. (a) Inferred occurrence and latitudinal extent of continental glaciation [Crowley, 1998]. (b) Oxygen isotopic composition ($\delta^{18}\text{O}$) of well-preserved carbonates [Veizer *et al.*, 1999, 2000]. The linear trend line of the data-set is shown as a dashed line. (c) Reconstructed Phanerozoic temperature anomalies (ΔT) from *Shaviv and Veizer* [2003] (blue line) and as corrected for pH by *Royer et al.* [2004] (red line).

Figure 8. Effect of Phanerozoic pH change on the interpretation of Phanerozoic temperature anomalies. (a) The results of carrying out the correction of *Royer et al.* [2004] using the reconstructed pH from Figure 6c. (b) The effect of first linearly detrending the pH curve before applying the pH– $\delta^{18}\text{O}$ correction to the $\delta^{18}\text{O}$ - ΔT relationship. In both panels the shaded band

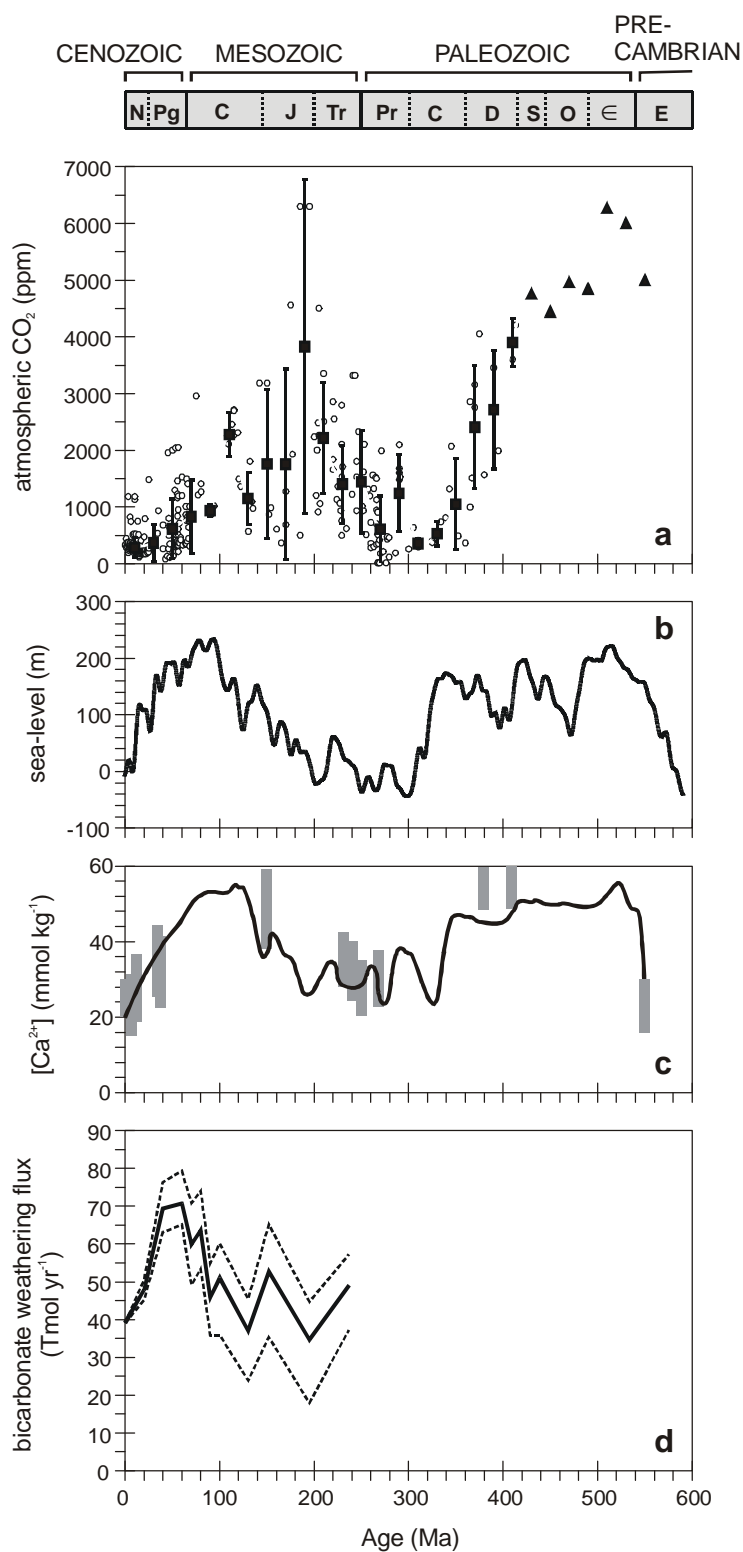
represents the uncertainty due to one standard deviation of the proxy CO₂ data. The horizontal dashed line represents the baseline with respect to modern.



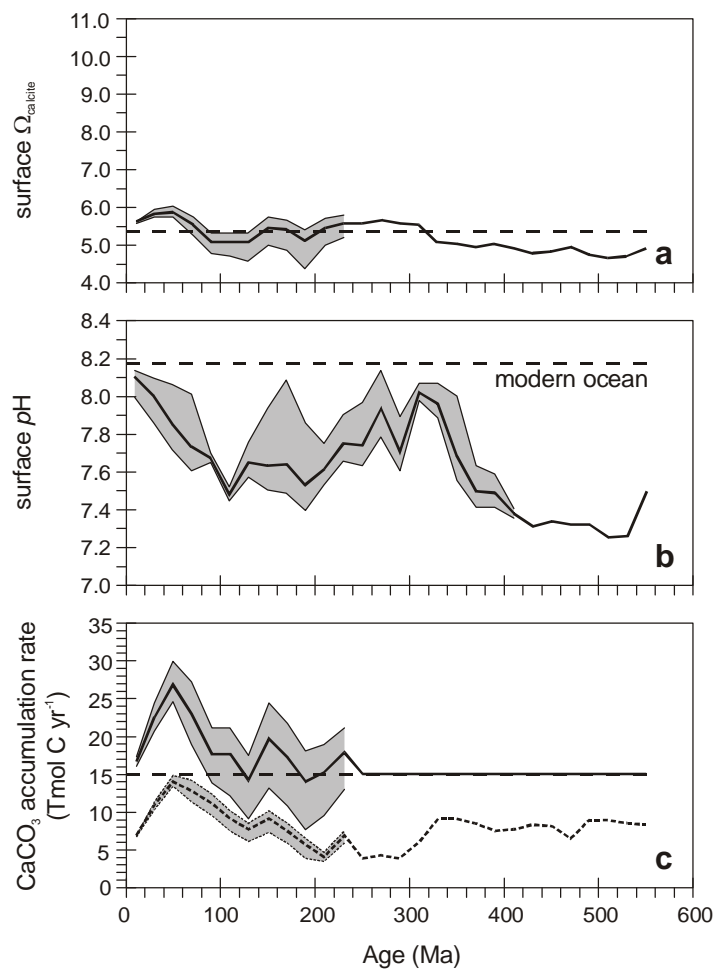
ridgwell_fig01



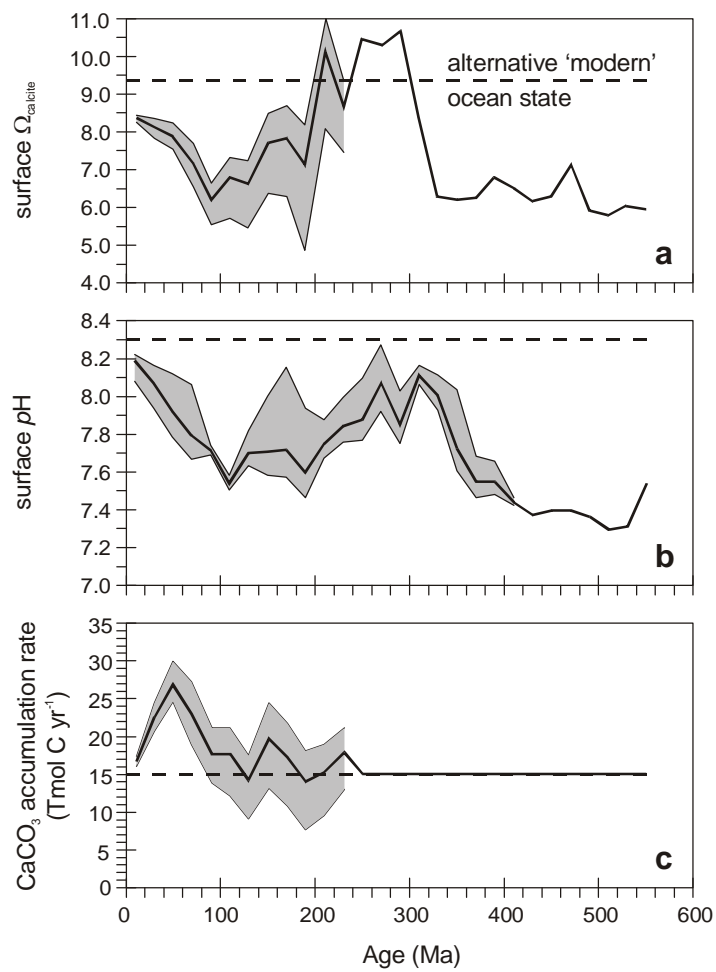
ridgwell_fig02



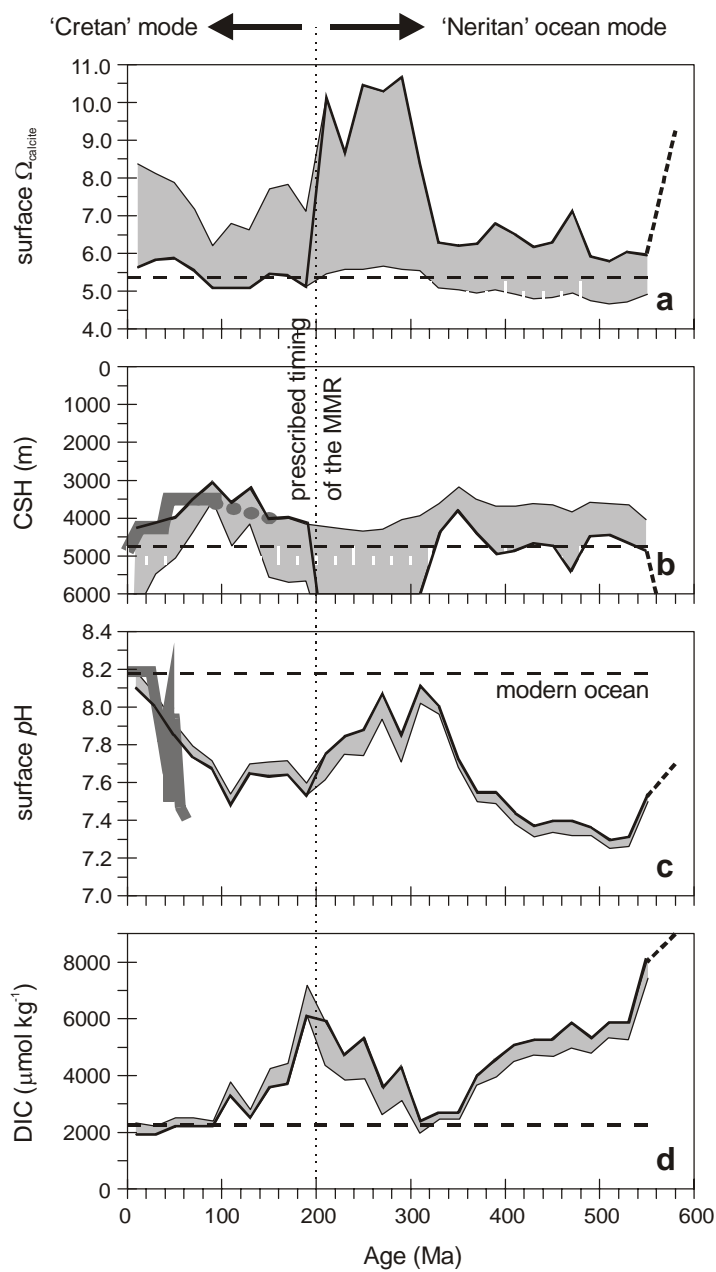
ridgwell_fig03



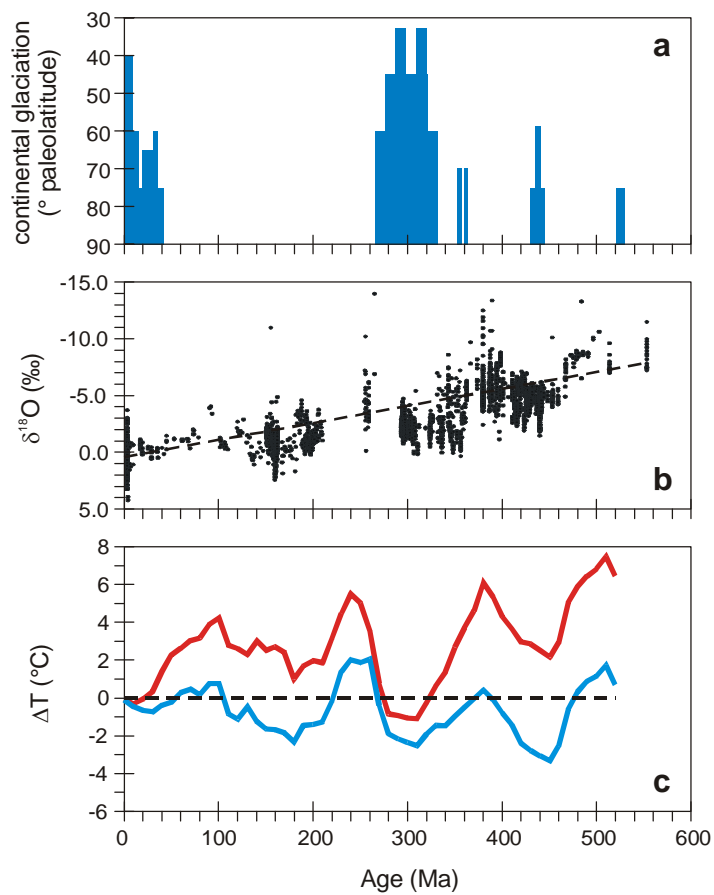
ridgwell_fig04



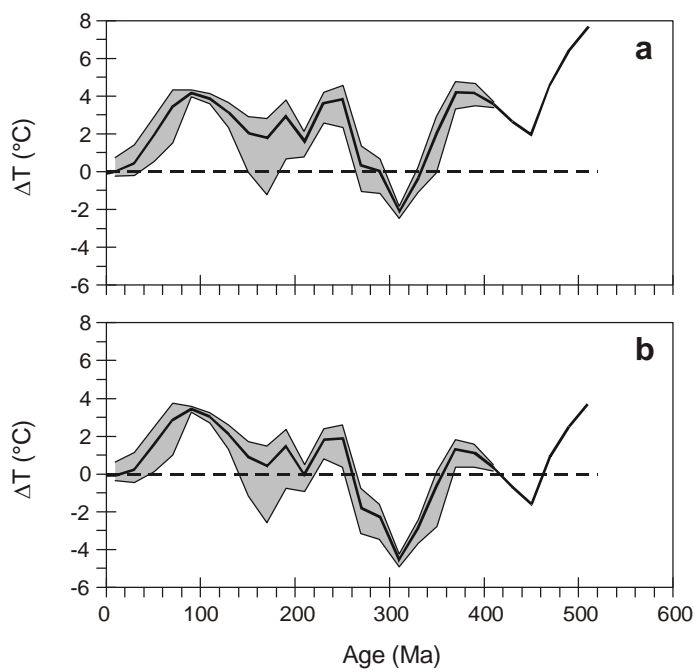
ridgwell_fig05



ridgwell_fig06



ridgwell_fig07



ridgwell_fig08